A Generalized Theory Explains the Anomalous Suns–V_{OC} Response of Si Heterojunction Solar Cells

Raghu Vamsi Krishna Chavali, Jian V. Li, *Senior Member, IEEE*, Corsin Battaglia, Stefaan De Wolf, Jeffery Lynn Gray, *Senior Member, IEEE*, and Muhammad Ashraful Alam, *Fellow, IEEE*

***Abstract*—Suns–V_{oc} measurements exclude parasitic series resistance effects and are, therefore, frequently used to study the intrinsic potential of a given photovoltaic technology. However, when applied to a-Si/c-Si heterojunction (SHJ) solar cells, the Suns–V_{oc} curves often feature a peculiar turnaround at high illumination intensities. Generally, this turn-around is attributed to extrinsic Schottky contacts that should disappear with process improvement. In this paper, we demonstrate that this voltage turnaround may be an intrinsic feature of SHJ solar cells, arising from the heterojunction (HJ), as well as its associated carrier-transport barriers, inherent to SHJ devices. We use numerical simulations to explore the full current–voltage (*J–V*) characteristics under different illumination and ambient temperature conditions. Using these characteristics, we establish the voltage and illumination-intensity bias, as well as temperature conditions necessary to observe the voltage turnaround in these cells. We validate our turnaround hypothesis using an extensive set of experiments on a high-efficiency SHJ solar cell and a molybdenum oxide (MoO_x) based hole collector HJ solar cell. Our work consolidates Suns–V_{oc} as a powerful characterization tool for extracting the cell parameters that limit efficiency in HJ devices.**

***Index Terms*—Amorphous semiconductors, current–voltage (*J–V*) characteristics, heterojunctions (HJs), modeling and simulation, silicon, solar cells or photovoltaics, Suns–V_{oc}.**

I. Introduction

EXCLUDING the extrinsic series resistance allows one to quantify the intrinsic power conversion potential of a solar cell. The study of illumination intensity (or, equivalently, associated short-circuit current density: J_{SC}) versus open-circuit voltage (V_{OC}) characteristic is one approach that is often used toward this goal, especially for c-Si solar cells [1], [2]. Sinton Instruments developed the Suns–V_{oc} characterization setup, capable of fast, automated measurements [3], [4]. Since then, the technique has been used to characterize other solar cells as well, such as a-Si/c-Si heterojunction (SHJ) [5] (see Fig. 1), Cu(In,Ga)Se_2, and $CuZnSnS_4$ [6] solar cells. This methodology is also finding new applications in real-time monitoring of series resistance degradation in outdoor photovoltaic arrays, as a proxy for overall degradation of panel efficiency [7].

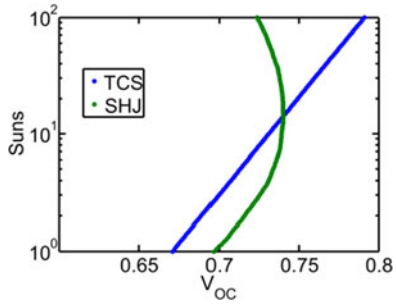

Fig. 1. Experimental Suns–V_{oc} measurements for typical TCS solar cell (blue), reproduced from [3] and SHJ solar cell (green), reproduced from [5] are presented.

For a homojunction c-Si solar cell (labeled hereafter as traditional c-Si solar cell, TCS), the blue curve in Fig. 1 shows that V_{OC} depends logarithmically on the illumination intensity (Suns, I). This is because the free-carrier generation scales with I, which in turn increases logarithmically the splitting of the quasi-Fermi levels, and thus, the voltage developed across the cell. At the open-circuit condition, the standard solar cell equation (obtained through the superposition of light and dark currents) can be rewritten to obtain

$$V_{\mathrm{OC}}\ (I) = \frac{nk_BT}{q}\ \log\left(\frac{J_{\mathrm{SC}}\ (I)}{J_0}\right) \tag{1}$$

where J_{SC} scales with I, and other symbols have their usual meanings.

In contrast, in heterojunction (HJ) solar cells [e.g., SHJ solar cells], the Suns–V_{oc} curve sometimes features a peculiar turnaround at high I (see the green curve in Fig. 1), inconsistent with (1). Such turnaround has sometimes been attributed to the formation of a parasitic front Schottky contact [4], [5], but the fundamental physics and the conditions under which it may occur are not yet fully understood.

In this study, we show that the origin of the turnaround for this class of devices need not be *extrinsic*; rather, the valence band offset at the HJ between the hole collector (i.e., the p/i a-Si

Manuscript received August 28, 2016; accepted October 19, 2016. This work was supported in part under the U.S.–India Partnership to Advance Clean Energy-Research (PACE-R) for the Solar Energy Research Institute for India and the United States (SERIIUS), funded jointly by the U.S. Department of Energy (Office of Science, Office of Basic Energy Sciences, and Energy Efficiency and Renewable Energy, Solar Energy Technology Program, under Subcontract DE-AC36-08GO28308 to the National Renewable Energy Laboratory, Golden, CO, USA) and the Government of India through the Department of Science and Technology under Subcontract IUSSTF/JCERDC-SERIIUS/2012 dated November 22, 2012.

R. V. K. Chavali was with the School of Electrical and Computer Engineering, Purdue University, West Lafayette, IN 47907 USA. He is now with Intel Corporation, Boise, ID 83707-0006 USA (e-mail: c.raghuvamsi@gmail.com).

J. V. Li is with the Department of Electrical Engineering, Texas State University, San Marcos, TX 78666 USA (e-mail: jianvli@txstate.edu).

C. Battaglia is with the Laboratory Materials for Energy Conversion, Empa—Swiss Federal Laboratories for Materials Science and Technology, 8600 Dübendorf, Switzerland (e-mail: corsin.battaglia@empa.ch).

S. De Wolf is with the KAUST Solar Center (KSC), King Abdullah University of Science and Technology (KAUST), Thuwal 23955-6900, Saudi Arabia (e-mail: stefaan.dewolf@kaust.edu.sa).

J. L. Gray and M. A. Alam are with the School of Electrical and Computer Engineering, Purdue University, West Lafayette, IN 47907 USA (e-mail: grayj@ecn.purdue.edu; alam@ecn.purdue.edu).

Color versions of one or more of the figures in this paper are available online at http://ieeexplore.ieee.org.

Digital Object Identifier 10.1109/JPHOTOV.2016.2621346

stack) and base (n c-Si), *intrinsic* to an SHJ solar cell, can explain this anomalous feature as well. We find that this HJ hypothesis is consistent with peculiarities observed in light *J–V* characteristics reported in earlier works [8], [9]. Fundamentally, the turnaround is dictated by the HJ band offset, which is controlled by a combination of intensity, temperature, and bias conditions.

Furthermore, this study suggests that the technique, when appropriately interpreted, can be used to obtain a broad range of information about solar cells. For example, the HJ theory presented here is consistent with our earlier work on dark and light *J–V* [8], impedance spectroscopy, and *C–V* analysis [10] of SHJ solar cells. Therefore, the Suns–$V_{\rm oc}$ technique can be used, in combination with other techniques, to extract device parameters, such as the HJ band offset (ΔE_V), surface potential (ϕ_N), etc. We also explain how the Suns-Photovoltage curves can be used to generalize the Suns–$V_{\rm oc}$ measurement at various bias conditions to help analyze the above features in a systematic and consistent manner. Finally, we validate our HJ hypothesis using experiments on two HJ device types, namely, a "standard" high-efficiency SHJ and a substoichiometric molybdenum oxide (MoO_x)-based hole collector HJ device, reported in [11].

II. Physics of Intensity and Temperature Response

A. Validity of the Principle of Superposition

Here, we provide the rationale for our HJ hypothesis by studying the necessary conditions for SHJ solar cells to satisfy (1). In any solar cell, regardless of whether it follows the superposition principle or not, the total current ($J_{\rm Tot}$) at a given intensity (I), bias (V), and temperature (T) can be written as [12]

$$J_{\rm Tot}\ (I,V,T) = J_{\rm Photo}\ (I,V,T) + J_{\rm Inj}\,(I,V,T) \quad (2)$$

where $J_{\rm Photo}$ is the total current density due to the photogenerated carriers, and $J_{\rm Inj}$ is the total current density due to diode-injected carriers. For a typical TCS solar cell, it is possible to simplify (2) by making the following two assumptions.

1) The diode injection current density $[J_{\rm Inj}(I,V,T)]$ is independent of the illumination intensity and is equal to the dark current density $[\ J_{\rm Inj} = J_{\rm Dark}\ (V,T)]$.
2) The photocurrent density $[J_{\rm Photo}(I,V,T)]$ is independent of the operating voltage and temperature so that $J_{\rm Photo} = J_{\rm SC}\ (I)$.

With these assumptions, (2) simplifies to the more familiar expression, namely

$$J_{\rm Tot}\ (I,V,T) = J_{\rm SC}\ (I) + J_{\rm Dark}\,(V,T)\,. \quad (3)$$

Equation (3) defines the "principle of superposition" [1], which states that the total current of a solar cell can be obtained as a superposition of the photocurrent measured under short-circuit conditions $[J_{\rm SC}(I)]$ and the dark *J–V* characteristics $[J_{\rm Dark}(V,T)]$. Using the diode equation for dark current, we can rewrite (3) as

$$J_{\rm Tot}\ (I,V,T) = J_{\rm SC}\ (I) + J_0\,(T)\left[e^{\frac{q\,(V\,-J_{\rm Tot}R)}{n\,k_B\,T}} - 1\right]. \quad (4)$$

At open-circuit conditions ($J_{\rm Tot} = 0$), (4) reduces to (1), which anticipates the blue curve in Fig. 1, based on experimental data from c-Si cells. Furthermore, Fig. 2(a) shows the numerically simulated room temperature *J–V* response at different I for a typical TCS solar cell [see Table II in the Appendix for simulation parameters]. From such curves, one can construct theoretical Suns–$V_{\rm oc}$ curves, as in Fig. 1, by plotting $V_{\rm oc}$ of each of these curves against the corresponding intensity (I). From this, it is obvious that a cell that obeys the superposition principle [see (3) and (4)] *will not* show a turnaround in the Suns–$V_{\rm oc}$ curve. However, if a homojunction cell contains a parasitic Schottky contact, its *J–V* characteristics are known to deviate from the superposition principle [1]. In addition, it shows a turnaround in Suns–$V_{\rm oc}$ characteristics [4].

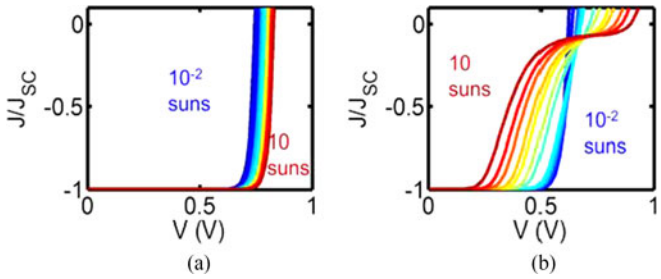

Fig. 2. Numerically simulated intensity-dependent normalized *J–V* curves of (a) a typical TCS solar cell and (b) HJ-limited SHJ solar cell are shown.

Considering the case of SHJ solar cells, it is well known that the superposition principle does not hold *per se* [8], [12], because the device often violates the low-level injection assumption of the superposition principle [1]. In addition, turnaround in the Suns–$V_{\rm oc}$ curve is often observed for this device class. This raises the question if the two phenomena are interlinked. With the two assumptions leading to (3) being invalid in the SHJ case, its *J–V* characteristics cannot be described by a simple analytical formula similar to (4). Instead, numerical simulation must be used to gain insight into its underlying operation principles. Notably, under certain temperature and illumination conditions, such a numerical simulation of the normalized *J–V* response (see Fig. 2(b), based on simulation parameters in Table III in Appendix) exhibits a strong S-shaped behavior at high I, significantly deviating from the assumptions of the superposition principle [the physical origin of these features is discussed in Section II-B]. In turn, Suns–$V_{\rm oc}$ curves constructed from such a family of *J–V* curves exhibit the turnaround at high I. Thus, it is not a surprise that (1) is not always valid for this type of solar cell.

Based on this correlation between the Suns–$V_{\rm oc}$ turnaround and the occurrence of S-shaped *J–V* characteristics, in this paper, we will answer the following three questions quantitatively.

1) How does the HJ, which is intrinsic to SHJ device, define the shape of *J–V* characteristics?
2) Under what measurement conditions (intensity, temperature) do S-shaped *J–V* curves arise?
3) Finally, what additional information can the Suns–photovoltage curve (obtained at voltages other than at open circuit) provide that can help interpret the performance of the cell?

In the following sections, first, we investigate questions 1 and 2 [see Section II-B] using numerical simulations. Based on the theory developed in Section II-B, we construct the Suns–photovoltage curves to answer question 3 [see Section II-C].

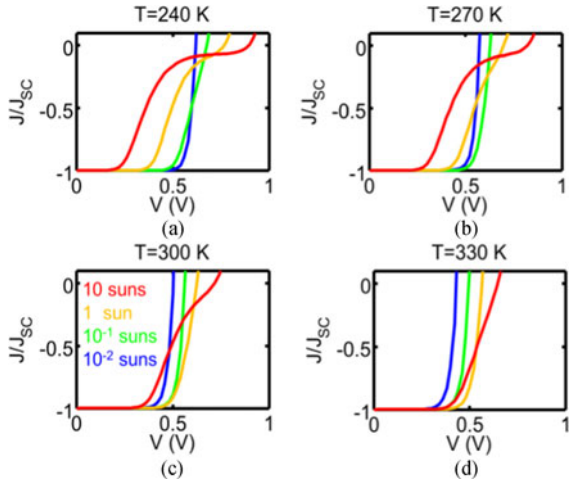

Fig. 3. (a) Simulated normalized *J–V* characteristics under different intensity conditions at temperature conditions (a) 240 K, (b) 270 K, (c) 300 K, and (d) 330 K indicate the temperature and intensity dependence of the S-shaped curve.

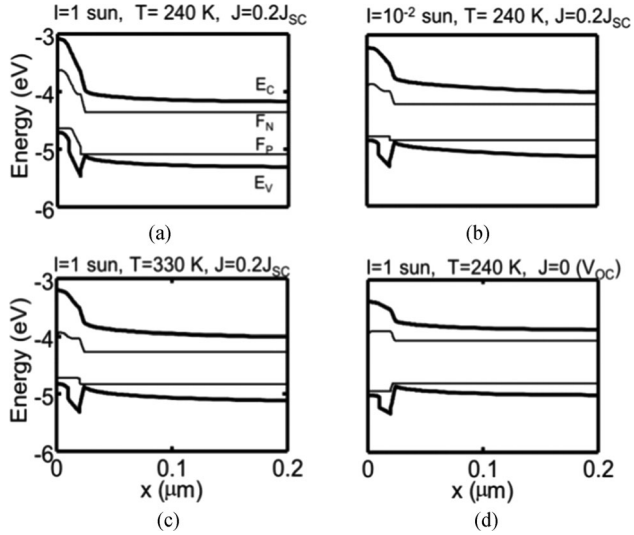

Fig. 4. Energy band diagrams, including quasi-Fermi levels (F_N and F_P), under different stimuli are presented. The collection of photocarriers is impeded in (a). In (b), intensity is reduced from (a). In (c), temperature is increased from (a). In (d), bias is increased from (a).

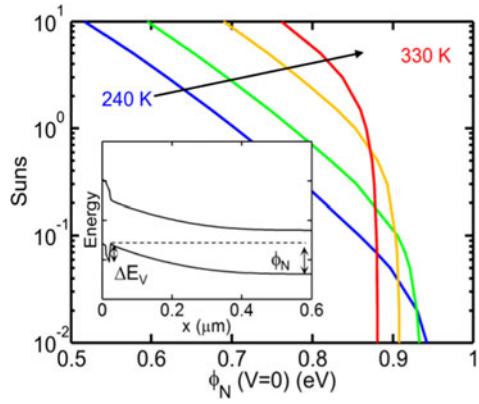

Fig. 5. Surface potential at 0 V (ϕ_N ($V = 0$ V)) is plotted against intensity (Suns) at different temperature conditions. (Inset) Equalibrium energy band diagram indicating ϕ_N and ΔE_V is presented.

B. Temperature and Intensity Dependencies of Light J–V Characteristics

In this section, we explore the HJ physics of T- and I-dependent light *J–V* characteristics. As we will see, T and I have correlated effects on the *J–V* characteristics. The electrostatics of the device, which is a function of I, T, and V, dictates the occurrence of the S-shaped light *J–V* characteristic. It is important to study the effects of I, T, and V together, because experiments with single stimulus (I or T or V) may not probe all the electrostatic conditions in the solar cell. Thus, studying them together can help identify the necessary conditions to observe the S-shaped *J–V* curve and the turnaround in Suns–V_{oc}. We have used the drift-diffusion simulator ADEPT 2.1 [13] for numerical simulation of the cell performance.[1] The input parameters are summarized in Table III in the Appendix.

The normalized light *J–V* curves for different I and T are presented in Fig. 3(a)–(d). There are two immediate observations that can be made from this family of *J–V* curves. First, at a given T [say $T = 240$ K; see Fig. 3(a)], increasing I causes an early onset of the S-shaped curve. Second, for a given I [say at 1 sun in Fig. 3(a)–(d)], increasing T eliminates the S-shaped curve. Thus, the general trends indicate opposite effects of T and I.

The reduced terminal voltage with increasing I (or decreasing T) is best explained by analyzing the quasi-Fermi levels within the device for a given current density [e.g., $J = 0.2J_{SC}$; see Fig. 4(a)–(c)]. As T is reduced (and/or I is increased), the hetero-barrier at the a-Si/c-Si interface begins to impede the collection of photogenerated holes, especially at sufficiently high forward bias. Therefore, the hole quasi-level (F_p) must drop significantly beyond the a-Si/c-Si interface [see Fig. 4(a)] so that the additional field can extract the carriers from the "inversion region" formed at the c-Si/a-Si interface. This internal drop ($\Delta F_p/q$) subtracts from the ideal photovoltage and reduces the terminal voltage developed across the cell, resulting in an S-shaped curve. As the bias approaches V_{oc}, the carrier recombination compensates the carrier generation, and hence, the net current is zero. Here, F_P is essentially flat in c-Si and a-Si layers [see Fig. 4(d)].

To appreciate these relationships intutively, one must first understand the origin of S-shaped light *J–V* and its correlations to dark *J–V* [8], [14]. Briefly, this is due to the drop in hole collection efficiency attributed to the valence band offset at the a-Si/c-Si HJ (ΔE_V; see the inset in Fig. 5), which acts as an energetic barrier for collection of photogenerated holes from the c-Si base [15].

One can also explain enhanced S-shaped curves with I and T by analyzing the photocollection properties of the HJ. First, at constant T, increasing I increases the density of photogenerated carriers in the c-Si absorber. This, in turn, affects the junction electrostatics, causing a reduction in surface potential (i.e., band bending, ϕ_N; see the inset of Fig. 5). Under these conditions, the photogenerated holes must surmount a higher effective valence

[1]Due to carrier freeze-out effects, even commercial drift-diffusion simulators (such as the one used in this study) have convergence limitations at very low temperatures. Therefore, the simulation results close to the freeze-out regime may not be reliable. Fortunately, given the broad range of experimental data, we can consistently explain the relevance of HJ for Sun–V_{oc} measurements by analyzing device physics starting from a slightly higher temperature (e.g. 240 K).

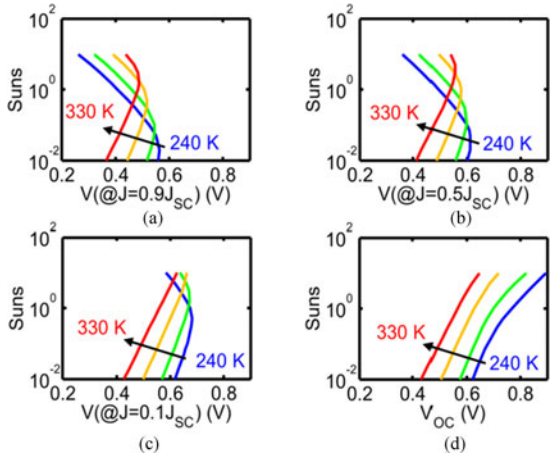

Fig. 6. Suns–photovoltage curves for different temperatures at different current density levels: (a) $J = -0.9J_{SC}$, (b) $J = -0.5J_{SC}$, (c) $J = -0.1J_{SC}$, and (d) V_{OC} conditions ($J = 0$) are presented. These curves indicate the evolution of turnaround from high-current conditions to the open-circuit condition.

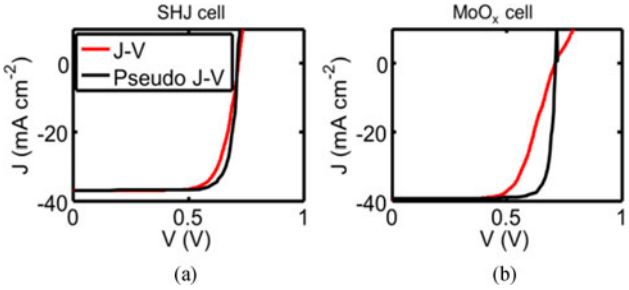

Fig. 7. Experimental *J–V* characteristics of (a) SHJ and (b) MoO_x cells at STC are plotted. The pseudo *J–V* obtained from standard Suns–V_{OC} is also plotted here.

TABLE I
PERFORMANCE CHARACTERISTICS OF SHJ CELL AND MoO_x CELL AT STC

Cell Name	J_{SC} (mA·cm^{-2})	V_{OC} (V)	FF (%)	η (%)	Pseudo η (%)
SHJ	37.1	716	75.9	20.2	21.8%
MoO_x	39.4	711	67.2	18.8	23.9%

band barrier (compared with the low *I* condition), resulting in an early onset of the S-shaped curve at high *I*. Next, to explain the T dependence, we note that at a given I, the photogeneration rate of carriers is constant, whereas carrier collection across the HJ interface is thermally activated (tunneling through a-Si layers, which has a weak temperature activation, is assumed to be negligible here). Thus, at lower T, a larger fraction of the photogenerated carriers cannot cross the HJ barrier, causing a "carrier pile-up" near the junction. This changes the junction electrostatics causing a reduction in ϕ_N, which further impedes the collection efficiency, resulting in the early onset of an S-shaped curve at low T. Note that ϕ_N increases with reduced temperature at very low intensities (e.g., 10^{-2} suns in Fig. 5), which is consistent with the expectation of Fermi-level change with temperature in the dark.

To summarize, we find that early onset of the S-shaped *J–V* may either be triggered by higher *I* or lower *T,* or both. The above discussion may be quantified by plotting the surface potential in c-Si (ϕ_N) at short-circuit conditions in Fig. 5. As expected, for a given T, increasing I reduces ϕ_N. Conversely, at a given I, lowering T reduces ϕ_N. These curves will quantify the shapes of Suns–photovoltage and Suns–V_{oc} curves to be discussed next.

C. Suns–Photovoltage Versus Suns–V_{oc} Curves

Using the *J–V* characteristics in Fig. 3(a)–(d), we construct the Suns–photovoltage curves for different T conditions and at different current densities in Fig. 6(a)–(d). For example, to obtain the blue curve in Fig. 6(a) (at $T = 240$ K), we read the voltage (V) at $J = -0.9J_{SC}$ for each I from Fig. 3(a) (for $T = 240$ K) and plot it against the corresponding I. Note that the Suns–photovoltage curves can be constructed at any J, varying between short- and open-circuit conditions. Here, we chose to construct the Suns–photovoltage curves at $J = -0.9J_{SC}$, $J = -0.5J_{SC}$, $J = -0.1J_{SC}$, and $J = 0$ (i.e., at V_{oc}) in Fig. 6(a)–(d) to systematically analyze the effects of I, V, and T on the Suns–photovoltage curves of this specific simulated HJ device, as well as to investigate the operating conditions where the superposition principle fails.

In Fig. 6(a) (plotted at $J = -0.9J_{SC}$), the hole collection and injection at the front contact is the major contributor for the total current density. For low intensities, the photovoltage is purely dictated by the splitting of the quasi-Fermi levels, and the device obeys the superposition principle [i.e., (1)]. However, for higher intensities, photovoltage turnaround occurs. Under these conditions, junction electrostatics and, thus, ϕ_N (see Fig. 5) dictate the hole collection. In addition, considering the full dataset given in Fig. 6(a)–(d), the turnaround is stronger at higher current density [$J = -0.9J_{SC}$; see Fig. 6(a)] while absent close to open-circuit conditions [see Fig. 6(d)] [16]. This is because, close to open-circuit condition, no external current is flowing; therefore, barriers can have no effect on the characteristics.

The detailed numerical simulation suggest that the turnaround in Suns–photovoltage curves can be an indicator for the presence of an intrinsic barrier (due to the HJ interface discontinuity) to charge collection. It may either be triggered by higher *I* or lower *T* and is prominent closer to maximum power point and disappears as we approach V_{oc}. Thus, we note that the turnaround can be caused by two quite different phenomena namely—HJ barriers (discussed in this work) and a Schottky barrier due to workfunction mismatch of contacting materials [4], [5]. We will compare these theoretical predictions of this work against experimental data to see if the interpretation of Suns–V_{oc} turnaround is justified.

III. EXPERIMENTAL SETUP AND VALIDATION

A. Experimental Setup

To explore the validity of HJ theory developed in Section II, I- and T-dependent *J–V* measurements are carried out on a "standard" high-quality SHJ solar cell, featuring its p-type a-Si hole collector at the front of the device, as well as a similar cell, where a MoO_x hole collector was used (consisting of an intrinsic a-Si buffer layer, capped with a MoO_x film, and referred to as MoO_x cell here). The fabrication details are presented in [11] and [17].

The SHJ cell does not show an S-shape in its light *J–V* characteristic at room temperature under 1-sun illumination (standard test conditions—STC) [see Fig. 7(a)]. Thus, the fill factor (FF) of the device is relatively high (i.e., 75.9%, as summarized in Table I). The light *J–V* curve closely follows the pseudo

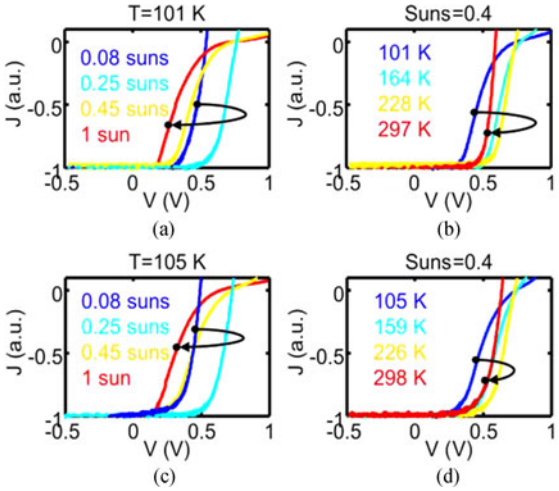

Fig. 8. Experimental normalized *J–V* characteristics of a SHJ cell for different (a) intensity conditions at $T = 101$ K and (b) temperature conditions at Suns $= 0.4$ are plotted. The corresponding *J–V* characteristics of a MoO_x cell for different (c) intensity conditions at $T = 105$ K and (d) temperature conditions at Suns $= 0.4$ are plotted. Arrows indicate increasing Suns or T.

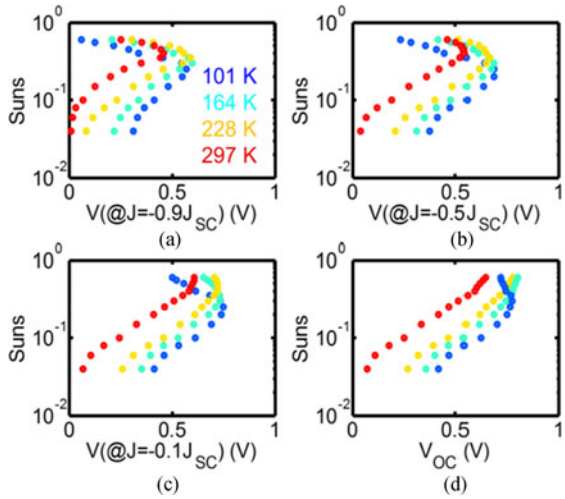

Fig. 9. Experimental Suns–photovoltage curves for standard SHJ cell at different temperatures and $J = -0.9J_{SC}$, $J = -0.5J_{SC}$, $J = -0.1J_{SC}$, and V_{OC} conditions ($J = 0$) are plotted in (a)–(d), respectively.

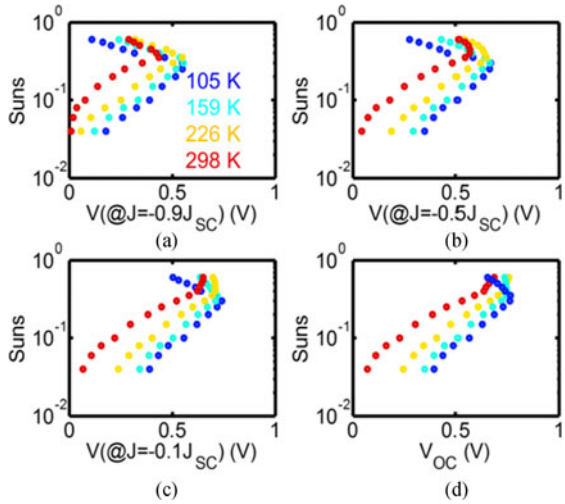

Fig. 10. Experimental Suns–photovoltage curves for MoO_x cell at different temperatures and $J = -0.9J_{SC}$, $J = -0.5J_{SC}$, $J = -0.1J_{SC}$, and V_{OC} conditions ($J = 0$) are plotted in (a)–(d), respectively.

J–V curve (obtained from the standard Suns–V_{oc} measurement [3], [4]), with the small deviation attributed to the series resistance. The pseudo efficiency for the cell is 21.8% (obtained from pseudo *J–V*), suggesting that the device does not suffer from HJ bottleneck at STC. The MoO_x cell, which has a more transparent window layer (MoO_x, with typical bandgap of 3.3eV), minimizes the parasitic absorption by the contact layer. As a result, J_{SC} for the MoO_x cell is higher than that of the SHJ cell, as shown in Table I. Although this specific MoO_x cell has a potential to achieve an efficiency of 23.9% (obtained from pseudo *J–V*) through J_{SC} improvements, the actual efficiency is limited to 18.8% due to FF loss attributed to S-shaped light *J–V* [see Fig. 7(b) and Table I]. Our hypothesis is that that the S-shape of the light *J–V* results from band misalignment at the front contact, as discussed in the following sections.

These solar cell devices were placed on the cold finger of a Janis CCS-350 closed-cycle helium-cooled cryostat. The temperature of the device, measured from a silicon diode sensor placed directly on top of the device, was lowered from ∼300 to ∼100 K in steps of 10 K. Note that the lower temperature limit (∼100 K) is chosen to ensure complete dopant ionization in c-Si [18]. After stabilizing at each temperature, the *J–V* characteristics were measured in the dark and under illumination using a Keysight B2912A source-measurement unit. The light intensity was modulated by a series of neutral-density filters inserted between an AM1.5G solar simulator (Newport 96000) and the device under test.

B. Experimental Validation

The J_{sc}-normalized *J–V* curves for the SHJ and MoO_x cell are presented in Fig. 8(a), (b) and (c), (d), respectively. We observe in Fig. 8(a) and (c) that at a given T, increasing I indeed causes early onset of the S-shape in the light *J–V* characteristics for both types of cells. This is due to the enhanced HJ offset barrier for hole collection at higher intensities, as discussed in Section II-B. Similarly, from Fig. 8(b) and (d), it can be observed that at a given I, decreasing T causes early onset of S-shaped light *J–V* curve. This is again due to enhanced hole collection HJ barrier for hole collection at lower temperature. *Furthermore, these results suggest that tunneling at the a-Si/c-Si interface is negligible [19] and confirm thermionic emission over the band offsets as dominating carrier transport mechanism [14].*

In addition, Suns–photovoltage curves are constructed from the *J–V* data of SHJ cell and MoO_x cell using the procedure described in Section II-C and presented in Figs. 9(a)–(d) and 10(a)–(d), respectively. Again, as expected, the voltage turnaround is observed to be strong under high I, low T, and is less prominent close to V_{oc}. Note that the turnaround at extremely low temperatures (∼ 100 K) is observed even close at V_{OC} conditions. This indicates that photocollection from the c-Si absorber (HJ barrier-dependent component) still dominates over the thermally suppressed injection current and additional carrier collection from the front a-Si layers, as opposed to what is observed at higher temperatures.

These results underline that, in essence, the experimental observation of turnaround in Suns–V_{oc} can be interpreted as a

direct consequence of the carrier emission over the HJ barrier. This barrier is strongly influenced by illumination intensity, temperature, and bias conditions. Thus, in a good SHJ device, it can be concluded that while the turnaround may be present at lower temperature, it may disappear under actual operation conditions.

IV. Discussion

In this paper, we have chosen to plot Suns–photovoltage curves at various T to study the conditions necessary to observe the voltage turnaround in Suns–$V_{\rm oc}$ curve. Alternatively, one could use T versus photovoltage curves at various I to explain the same phenomena. In fact, when T versus FF curve is plotted at 1-sun condition in [14], we observe that the corresponding features are in agreement with observations presented here.

Furthermore, we observe that the turnaround is present at very low temperature experimental Suns–$V_{\rm oc}$ characteristics [see Figs. 9(d) and 10(d)]. Presumably, this is due to the fact that dopant freeze-out occurs at higher temperatures in a-Si layers that the c-Si wafer. Thus, the effective doping in p-doped layers becomes simply too weak to support the electrical junction, especially at higher intensities. Additionally, at very low temperatures, the effect of intensity-dependent increase in cell temperature can become important [27]. It is known that increasing I increases the operating temperature of the cell ($T_{\rm op}$), especially at $V_{\rm oc}$, because the power dissipated ($P_{\rm diss}$) is equal to the input power ($P_{\rm in}$). This increase in temperature (at $V_{\rm oc}$) increases the overall recombination, reduces $V_{\rm oc}$ below the ideal case [predicted by (1)], and is reflected in the Suns–$V_{\rm oc}$ curve [3]. Note that this effect is more pronounced at lower temperature [at 105 K in this case; see Figs. 9(d) and 10(d)], because the relative increase in recombination compared with ideal [as predicted by (1)] is higher at lower temperature than higher temperature. Note that this self-heating effect may cause uncertainty in interpreting the effect of HJ from the Suns–$V_{\rm oc}$ results. Hence, one has to look at the more general Suns–photovoltage characteristics [see Figs. 9(a)–(c) and 10(a)–(c)] to analyze the HJ bottleneck in these devices.

To illustrate the self-consistency of the HJ theory in explaining a wide range of measurements, we use the extensive measurements of dark *J–V*, light *J–V*, and Suns–$V_{\rm oc}$ provided by Das *et al.* [21]. Based on the data presented in [21], we note the following for one (first) set of devices.

1) The dark *J–V* saturation occurs at medium bias.
2) The light *J–V* exhibits S-shaped characteristics.
3) The Suns–$V_{\rm oc}$ exhibits turnaround at high intensity.

On the other hand, for the second set of devices, we note the following.

1) The dark *J–V* saturation does not occur at medium bias.
2) The light *J–V* does not exhibit S-shaped characteristics.
3) The Suns–$V_{\rm oc}$ does not exhibit turnaround at high intensity.

These results indicate that the first set of devices could be limited by HJ, while the second set is not, which is consistent with the HJ theory and results presented here and in [8].

In addition, we note that the discussion presented here does not exclude the possibility of *extrinsic* Schottky contact, rather, it explain how an *intrinsic* HJ itself can exhibit these features, even in the absence of Schottky barriers. Hence, one needs to be cautious about concluding the presence/absence of Schottky barrier or HJ simply based on Suns–$V_{\rm oc}$ measurement. Indeed, with regard to measurements that probe the carrier collection properties in solar cells, such as *J–V* and Suns–$V_{\rm oc}$, the signatures of HJ or Schottky contact are generally indistinguishable. This is because both these features suppress carrier collection and show similar output characteristics. Nevertheless, when analyzed self-consistently with other techniques, such as *C–V* [10], dark *J–V–T* [8], [22], impedance spectroscopy [10], [23], surface photovoltage [24], etc., one should be able to infer presence/absence of a Schottky contact for a specific process technology and recommend effective strategies for process improvement.

Finally, we note that the analysis serves as a diagnostic tool to understand the HJ bottlenecks in SHJ cells. In addition, for a cell manufacturer attempting to eliminate S-shape from light *J–V* curves present at the STC condition, this paper indicates that S-shape may be suppressed significantly at operating conditions (typical SHJ cell operating $T \sim$340 K $> T_{\rm STC}$ and I $\sim$ 0.2-0.9 suns $< I_{\rm STC}$), and therefore, the SHJ cell optimization space is simpler than conventionally assumed. *Hence, we emphasize the need for optimizing the cell at operating conditions rather than STC conditions.*

V. Conclusion

We have presented a comprehensive study of the role of HJ on the bias, temperature, and intensity-dependent collection properties of SHJ solar cells. The conclusions are as follows.

1) The turnaround in Suns–$V_{\rm oc}$ can be attributed to the intrinsic HJ at the a-Si/c-Si interface, introducing barriers for carrier transport. This HJ hypothesis is validated using experiments on SHJ solar cells. In addition, we conclude that a one-to-one correlation of Suns–$V_{\rm oc}$ turnaround to the Schottky barrier may not be accurate.
2) I and T have reciprocal effects on the turnaround in Suns–photovoltage and Suns–$V_{\rm oc}$ curves.
3) Exploring V-dependent Suns–photovoltage curves can help in further development of Suns–$V_{\rm oc}$ measurement technique when applied to complex device configurations.

Correctly interpreted, Suns–$V_{\rm oc}$ measurement is a powerful technique that complements other characterization techniques, such as dark/light *J–V* [8], [25], *C–V*, impedance spectroscopy [10] and, as a part of a "multiprobe" approach, can help characterize device-relevant interface parameters, such as the HJ band offset (ΔE_V), surface potential (ϕ), etc., in these type of devices. This analysis can also be applied to other thin-film HJ solar cells to better understand the transport and electrostatics-dependent bottlenecks in these devices.

Appendix

TABLE II
Numerical Simulation Input Parameters for a p-n Junction c-Si Cell

Properties	p-layer	n-layer
Thickness	3 um	200 um
Doping ($\rm cm^{-3}$)	$N_A = 5 \times 10^{18}$	$N_D = 5 \times 10^{15}$
Hole mobility ($\rm cm^2/Vs$)	300	430
Electron mobility ($\rm cm^2/Vs$)	1000	1230
Hole lifetime[1] (s)	10^{-4}	10^{-4}
Electron lifetime[1] (s)	10^{-4}	10^{-4}
Band gap (eV)	1.12	1.12
Electron affinities (eV)	4.05	4.05
Contact properties	Ohmic, $s_f = 10^2$ cm/s for minority carriers	

TABLE III
NUMERICAL SIMULATION INPUT PARAMETERS FOR SHJ SOLAR CELL

Properties	p-layer	i-layer	c-Si	i-layer	n-layer
Thickness	10 nm	10 nm	200 μm	10 nm	60 nm
Doping (cm^{-3})	$N_A = 1\times10^{19}$	–	$N_D = 5\times10^{15}$	–	$N_D = 10^{19}$
Hole mobility ($\mathrm{cm}^2/\mathrm{Vs}$)	1	2	340	2	2
Electron mobility ($\mathrm{cm}^2/\mathrm{Vs}$)	10	20	1100	20	20
Hole lifetime[1] (s)	–	–	10^{-4}	–	–
Electron lifetime [1] (s)	–	–	10^{-4}	–	–
Bandgap (eV)	1.62	1.8	1.1557	1.7	1.7
Electron affinities (eV)	3.9	3.9	4.05	3.9	3.9
Conduction Band Tail States	$N_{\mathrm{tail}} = 10^{19}$ cm^{-3}eV^{-1} $E_{\mathrm{tail}} = 0.05$ eV $C_h = 10^{-16}$ cm^{-2} $C_n = 10^{-16}$ cm^{-2}	$N_{\mathrm{tail}} = 10^{19}$ cm^{-3}eV^{-1} $E_{\mathrm{tail}} = 0.019$ eV $C_h = 10^{-16}$ cm^{-2} $C_n = 10^{-16}$ cm^{-2}	–	$N_{\mathrm{tail}} = 10^{19}$ cm^{-3}eV^{-1} $E_{\mathrm{tail}} = 0.019$ eV $C_h = 10^{-16}$ cm^{-2} $C_n = 10^{-16}$cm^{-2}	$N_{\mathrm{tail}} = 10^{19}$ cm^{-3}eV^{-1} $E_{\mathrm{tail}} = 0.05$ eV $C_h = 10^{-16}$ cm^{-2} $C_n = 10^{-16}$cm^{-2}
Valence band tail states	$N_{\mathrm{tail}} = 10^{19}$ cm^{-3}eV^{-1} $E_{\mathrm{tail}} = 0.1$ eV $C_h = 10^{-16}$ cm^{-2} $C_n = 10^{-16}$cm^{-2}	$N_{\mathrm{tail}} = 10^{19}$ cm^{-3}eV^{-1} $E_{\mathrm{tail}} = 0.049$ eV $C_h = 10^{-16}$ cm^{-2} $C_n = 10^{-16}$cm^{-2}	–	$N_{tail} = 10^{19}$ cm^{-3}eV^{-1} $E_{\mathrm{tail}} = 0.049$ eV $C_h = 10^{-16}$ cm^{-2} $C_n = 10^{-16}$cm^{-2}	$N_{\mathrm{tail}} = 10^{19}$ cm^{-3}eV^{-1} $E_{\mathrm{tail}} = 0.1$ eV $C_h = 10^{-16}$ cm^{-2} $C_n = 10^{-16}$cm^{-2}
Donor-like defects	$N_{t1} = 10^{16}$ cm^{-3} $E_{t1} - E_i = 0.31$ eV $\sigma_{t1} = 0.08$ eV $\tau_{p1} = 10^{-9}$ s $\tau_{n1} = 10^{-9}$ s $N_{t2} = 10^{18}$ cm^{-3} $E_{t2} - E_i = -0.26$ eV $\sigma_{t2} = 0.15$ eV $\tau_{p2} = 10^{-9}$ s $\tau_{n2} = 10^{-9}$ s	$N_{t1} = 5\times10^{15}$cm^{-3} $E_{t1} - E_i = 0.21$ eV $\sigma_{t1} = 0.08$ eV $\tau_{p1} = 2\times10^{-9}$ s $\tau_{n1} = 2\times10^{-9}$ s	–	$N_{t1} = 5\times10^{15}$cm^{-3} $E_{t1} - E_i = 0.21$ eV $\sigma_{t1} = 0.08$ eV $\tau_{p1} = 2\times10^{-9}$ s $\tau_{n1} = 2\times10^{-9}$ s	$N_{t1} = 10^{16}$ cm^{-3} $E_{t1} - E_i = 0.31$ eV $\sigma_{t1} = 0.08$ eV $\tau_{p1} = 10^{-9}$ s $\tau_{n1} = 10^{-9}$ s $N_{t2} = 10^{18}$ cm^{-3} $E_{t2} - E_i = -0.26$ eV $\sigma_{t2} = 0.15$ eV $\tau_{p2} = 10^{-9}$ s $\tau_{n2} = 10^{-9}$ s
Acceptor-like defects	$N_{t1} = 10^{16}$ cm^{-3} $E_{t1} - E_i = -0.21$ eV $\sigma_{t1} = 0.08$ eV $\tau_{p1} = 10^{-9}$ s $\tau_{n1} = 10^{-9}$ s	$N_{t1} = 5\times10^{15}$cm^{-3} $E_{t1} - E_i = 0.11$ eV $\sigma_{t1} = 0.08$ eV $\tau_{p1} = 2\times10^{-9}$ s $\tau_{n1} = 2\times10^{-9}$ s	–	$N_{t1} = 5\times10^{15}$cm^{-3} $E_{t1} - E_i = 0.11$ eV $\sigma_{t1} = 0.08$ eV $\tau_{p1} = 2\times10^{-9}$ s $\tau_{n1} = 2\times10^{-9}$ s	$N_{t1} = 10^{16}$ cm^{-3} $E_{t1} - E_i = -0.21$ eV $\sigma_{t1} = 0.08$ eV $\tau_{p1} = 10^{-9}$ s $\tau_{n1} = 10^{-9}$ s
Temperature-dependent E_G parameters[2]	–	–	$\alpha = 7.021\times10^{-4}$eVK^{-1} $\beta = 1108$ K	–	–
Contact properties			Ohmic contacts, $s_f = 10^7$ cm/s for both contacts		
a-Si/c-Si interface properties			$s_{\mathrm{intf}} = 500$ cm/s for both interfaces		

[1]SRH, Auger, and radiative recombination are included in the numerical models.

[2]To improve the accuracy of our simulations, we use Varshni model ($E_G = E_{G0} - \frac{\alpha T^2}{T+\beta}$) for c-Si bandgap estimation [26].

ACKNOWLEDGMENT

The authors would like to thank Prof. M. Lundstrom and Prof. P. Bermel, Purdue University, for fruitful discussions. The samples used in this work were fabricated at the École Polytechnique Fédérale de Lausanne, Neuchâtel, Switzerland. The measurements were conducted at the National Renewable Energy Laboratory, Golden CO, USA.

REFERENCES

[1] F. A. Lindholm, J. G. Fossum, and E. L. Burgess, "Application of the superposition principle to solar-cell analysis," *IEEE Trans. Electron Devices*, vol. ED-26, no. 3, pp. 165–171, Mar. 1979.

[2] R. J. Schwartz, M. S. Lundstrom, and R. D. Nasby, "The degradation of high-intensity BSF solar-cell fill factors due to a loss of base conductivity modulation," *IEEE Trans. Electron Devices*, vol. ED-28, no. 3, pp. 264–269, Mar. 1981.

[3] M. J. Kerr, A. Cuevas, and R. A. Sinton, "Generalized analysis of quasi-steady-state and transient decay open circuit voltage measurements," *J. Appl. Phys.*, vol. 91, no. 1, 2002, Art. no. 399.

[4] R. A. Sinton and A. Cuevas, "A quasi-steady-state open-circuit voltage method for solar cell characterization," in *Proc. 16th Eur. Photovoltaics Sol. Energy Conf.*, May 2000, pp. 1–4.

[5] M. Bivour, C. Reichel, M. Hermle, and S. W. Glunz, "Improving the a-Si: H(p) rear emitter contact of n-type silicon solar cells," *Sol. Energy Mater. Sol. Cells*, vol. 106, pp. 11–16, Nov. 2012.

[6] O. Gunawan, T. Gokmen, and D. B. Mitzi, "Suns-VOC characteristics of high performance kesterite solar cells," *J. Appl. Phys.*, vol. 116, no. 8, Aug. 2014, Art. no. 084504.

[7] M. G. Deceglie, T. J. Silverman, B. Marion, and S. R. Kurtz, "Real-time series resistance monitoring in PV systems without the need for I–V curves," *IEEE J. Photovoltaics*, vol. 5, no. 6, pp. 1706–1709, Nov. 2015.

[8] R. V. K. Chavali, J. R. Wilcox, B. Ray, J. L. Gray, and M. A. Alam, "Correlated nonideal effects of dark and light I–V characteristics in a-Si/c-Si heterojunction solar cells," *IEEE J. Photovoltaics*, vol. 4, no. 3, pp. 763–771, May 2014.

[9] M. W. M. van Cleef *et al.*, "Amorphous silicon carbide/crystalline silicon heterojunction solar cells: A comprehensive study of the photocarrier collection," *Jpn. J. Appl. Phys.*, vol. 37, no. 7, pp. 3926–3932, Jul. 1998.

[10] R. V. K. Chavali *et al.*, "Multiprobe characterization of inversion charge for self-consistent parameterization of HIT cells," *IEEE J. Photovoltaics*, vol. 5, no. 3, pp. 725–735, May 2015.

[11] C. Battaglia *et al.*, "Silicon heterojunction solar cell with passivated hole selective MoOx contact," *Appl. Phys. Lett.*, vol. 104, no. 11, Mar. 2014, Art. no. 113902.

[12] R. V. K. Chavali *et al.*, "The frozen potential approach to separate the photocurrent and diode injection current in solar cells," *IEEE J. Photovoltaics*, vol. 5, no. 3, pp. 865–873, May 2015.

[13] J. L. Gray *et al.*, "ADEPT 2.1," *nanoHub.org*, Mar. 2014. [Online]. Available: http://nanohub.org/resources/10913

[14] J. P. Seif *et al.*, "Amorphous silicon oxide window layers for high-efficiency silicon heterojunction solar cells," *J. Appl. Phys.*, vol. 115, no. 2, Jan. 2014, Art. no. 24502.

[15] J. P. Seif *et al.*, "Asymmetric band offsets in silicon heterojunction solar cells: Impact on device performance," *J. Appl. Phys.*, vol. 120, no. 5, Aug. 2016, Art. no. 054501.
[16] A. Tomasi *et al.*, "Transparent electrodes in silicon heterojunction solar cells: Influence on contact passivation," *IEEE J. Photovoltaics*, vol. 6, no. 1, pp. 17–27, Jan. 2016.
[17] J. Geissbühler *et al.*, "22.5% efficient silicon heterojunction solar cell with molybdenum oxide hole collector," *Appl. Phys. Lett.*, vol. 107, no. 8, Aug. 2015, Art. no. 081601.
[18] R. F. Pierret, *Advanced Semiconductor Fundamentals*, vol. 121. Boston, MA, USA: Addison-Wesley Longman, 1987, p. 221.
[19] A. Kanevce and W. K. Metzger, "The role of amorphous silicon and tunneling in heterojunction with intrinsic thin layer (HIT) solar cells," *J. Appl. Phys.*, vol. 105, no. 9, 2009, Art. no. 094507.
[20] M. A. Green, "General temperature dependence of solar cell performance and implications for device modelling," *Prog. Photovoltaics, Res. Appl.*, vol. 11, no. 5, pp. 333–340, Aug. 2003.
[21] U. Das *et al.*, "Investigation of hetero-interface and junction properties in silicon heterojunction solar cells," in *Proc. 35th IEEE Photovoltaics Spec. Conf.*, 2010, pp. 1358–1362.
[22] T. F. Schulze, L. Korte, E. Conrad, M. Schmidt, and B. Rech, "Electrical transport mechanisms in a-Si: H/c-Si heterojunction solar cells," *J. Appl. Phys.*, vol. 107, no. 2, 2010, Art. no. 023711.
[23] J. V. Li *et al.*, "Capacitance study of inversion at the amorphous-crystalline interface of n-type silicon heterojunction solar cells," *J. Appl. Phys.*, vol. 110, no. 11, 2011, Art. no. 114502.
[24] H. Angermann *et al.*, "Optimisation of electronic interface properties of a-Si:H/c-Si hetero-junction solar cells by wet-chemical surface pretreatment," *Thin Solid Films*, vol. 516, no. 20, pp. 6775–6781, Aug. 2008.
[25] R. V. K. Chavali, J. R. Wilcox, B. Ray, J. L. Gray, and M. A. Alam, "A diagnostic tool for analyzing the current-voltage characteristics in a-Si/c-Si heterojunction solar cells," in *Proc. 39th IEEE Photovoltaics Spec. Conf.*, 2013, vol. 1, pp. 0652–0657.
[26] Y. P. Varshni, "Temperature dependence of the energy gap in semiconductors," *Physica*, vol. 34, no. 1, pp. 149–154, Jan. 1967.
[27] G. Nogay *et al.*, "Nanocrystalline Silicon Carrier Collectors for Silicon Heterojunction Solar Cells and Impact on Low-Temperature Device Characteristics," in IEEE Journal of Photovoltaics, vol. 6, no. 6, pp. 1654–1662, Nov. 2016.

Raghu Vamsi Krishna Chavali received the B.E. (Hons.) degree in electrical and electronics engineering from Birla Institute of Technology and Science, Pilani, India, in 2009 and the M.S. and Ph.D. degrees in electrical and computer engineering from Purdue University, West Lafayette, IN, USA, in 2011 and 2016, respectively.

He then joined Intel Corporation, where he is working on next-generation memory products as a Reliability R&D Engineer. He has published papers in seven journals and more than ten conference papers during his Ph.D. work. His research interests include modeling, simulation, and characterization of semiconductor devices. He also studies the transport properties in amorphous materials.

Dr. Chavali received Best Poster Award in the area of fundamentals and new concepts at the 40th IEEE Photovoltaic Specialist Conference in 2014.

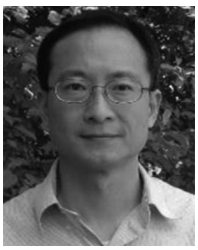

Jian V. Li (M'99–SM'14) received the B.E. degree in modern physics from the University of Science and Technology of China, Hefei, China, in 1995 and the Ph.D. degree in electrical engineering from the University of Illinois at Urbana-Champaign, Champaign, IL, USA, in 2005.

From 1997 to 2002, he was a Hardware Engineer with National Instruments. From 2004 to 2007, he was a Research Engineer with the Jet Propulsion Laboratory, Pasadena, CA, USA. From 2007 to 2015, he was a Research Scientist with the National Renewable Energy Laboratory. Since 2015, he has been with Texas State University, San Marcos, TX, USA, as an Associate Professor of physics and of materials science engineering and commercialization. His research interests include the electrical properties of semiconductor materials and devices, especially defects, interfaces, and recombination.

Corsin Battaglia received his Ph.D. degree in solid-state physics from the Université de Neuchâtel, Switzerland, in 2008.

He was subsequently a Postdoctoral Researcher at the Ecole Polytechnique Fédérale de Lausanne, Switzerland. From 2012 to 2014, he was a Postdoctoral Researcher at the University of California at Berkeley and Lawrence Berkeley National Laboratory. Since 2014, he is Head of the Laboratory at the Swiss Federal Laboratories for Materials Science and Technology (Empa), Dübendorf, Switzerland, in 2014, where he is directing the Laboratory Materials for Energy Conversion, focusing on materials and devices innovation for renewable energy conversion and storage technologies.

Stefaan De Wolf received the Ph.D. degree in electrical engineering from the Katholieke Universiteit Leuven, Belgium, in 2005.

During Ph.D. research, he was also affiliated with imec, Heverlee, Belgium, where he worked on crystalline silicon solar cells. From 2005 to 2008, he was with the National Institute of Advanced Industrial Science and Technology, Tsukuba, Japan, investigating silicon heterojunction structures and devices. In 2008, he joined the Photovoltaics and Thin-Film Electronics Laboratory, Ecole Polytechnique Federale de Lausanne, Switzerland, as a Team Leader for its activities on high-efficiency silicon solar cells. Since September 2016, he is an Associate Professor at King Abdullah University of Science and Technology, Thuwal, Saudi Arabia.

Jeffery Lynn Gray (SM'11) received the B.S. degree in physics and mathematics from the University of Wisconsin, River Falls, WI, USA, in 1976 and the M.S.E.E. and Ph.D. degrees in electrical engineering from Purdue University,West Lafayette, IN, USA, in 1978 and 1982, respectively.

He is currently an Associate Professor of electrical and computer engineering and serves as the Undergraduate Coordinator for the School of Electrical and Computer Engineering, Purdue University. He specializes in the modeling of photovoltaic devices and systems. He has authored or coauthored more than 90 journal and conference papers.

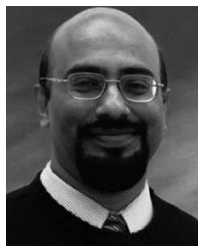

Muhammad Ashraful Alam (M'96–SM'01–F'06) received the B.S.E.E. degree from Bangladesh University of Engineering and Technology, Dhaka, Bangladesh, in 1988; the M.S. degree from Clarkson University, Potsdam, NY, USA, in 1991; and the Ph.D. degree from Purdue University, Lafayette, IN, USA, in 1994, all in electrical engineering.

He is currently the Jai N. Gupta Professor of electrical and computer engineering with the School of Electrical Engineering and Computer Science, Purdue University, where his research and teaching focus on physics, simulation, characterization, and technology of classical and novel semiconductor devices. From 1995 to 2001, he was with Bell Laboratories, Lucent Technologies, Murray Hill, NJ, USA, as a member of Technical Staff with the Silicon ULSI Research Department. From 2001 to 2003, he was a Distinguished Member of Technical Staff and the Technical Manager of the IC Reliability Group, Agere Systems, Murray Hill. In 2004, he joined Purdue University. His current research interests include stochastic transport theory of oxide reliability, transport in nanonet thin-film transistors, and nanobiosensors. He has published more than 200 papers in international journals and has presented many invited and contributed talks at international conferences.

Dr. Alam received the IRPS Best Paper Award in 2003 and the Outstanding Paper Award in 2001, both for his work on gate oxide reliability, and the IEEE Kiyo Tomiyasu Award for his contributions to device technology for communication systems.